

## Two-dimensional terahertz magnetic resonance spectroscopy of collective spin waves

Jian Lu<sup>1,\*</sup>, Xian Li<sup>1,\*</sup>, Harold Y. Hwang<sup>1</sup>, Benjamin K. Ofori-Okai<sup>1</sup>, Takayuki Kurihara<sup>2</sup>, Tohru Suemoto<sup>2</sup> and Keith A. Nelson<sup>1</sup>

<sup>1</sup>Department of Chemistry, Massachusetts Institute of Technology, Cambridge, MA 02139, USA.

<sup>2</sup>Institute for Solid State Physics, The University of Tokyo, Kashiwa, Chiba 277-8581, Japan.

\*These authors contributed equally to this work.

Corresponding author: K.A.N. ([kanelson@mit.edu](mailto:kanelson@mit.edu)).

**Nonlinear manipulation of nuclear and electron spins is the basis for all advanced methods in magnetic resonance including multidimensional nuclear magnetic and electron spin resonance spectroscopies<sup>1, 2</sup>, magnetic resonance imaging, and in recent years, quantum control over individual spins<sup>3</sup>. The methodology is facilitated by the ease with which the regime of strong coupling can be reached between radiofrequency or microwave magnetic fields and nuclear or electron spins respectively, typified by sequences of magnetic pulses that control the magnetic moment directions<sup>1,2,3</sup>. The capabilities meet a bottleneck, however, for far-infrared magnetic resonances characteristic of correlated electron materials, molecular magnets<sup>4</sup>, and proteins<sup>5</sup> that contain high-spin transition metal ions. Here we report the development of two-dimensional terahertz magnetic resonance spectroscopy and its use for direct observation of the nonlinear responses of collective spin waves (magnons). The spectra show magnon spin echoes and 2-quantum signals that reveal pairwise correlations between magnons at the Brillouin zone center. They also show resonance-enhanced second-harmonic and difference-frequency signals. Our methods are readily generalizable to multidimensional magnetic resonance spectroscopy and nonlinear coherent control of terahertz-frequency spin systems in molecular complexes, biomolecules, and materials.**

Electron spin resonances (ESR) in the terahertz (THz) frequency region can reveal rich information content in chemistry, biology, and materials science<sup>1, 2, 4, 5</sup>. In molecular complexes and proteins, THz-frequency zero-field splittings (ZFS) of high-spin transition metal and rare earth ions show exquisite sensitivity to ligand geometries, providing mechanistic insight into catalytic function<sup>5</sup>. With strong applied magnetic fields ( $\sim 10$  tesla), resonances of unpaired electron spins in molecular complexes can be shifted from the usual microwave regime into the THz range, drastically improving the resolution of spectral splittings due to interactions with nuclear spins that reveal molecular structure<sup>2</sup>. In many ferromagnetic (FM) and antiferromagnetic (AFM) materials, intrinsic magnetic fields in the same range put collective spin wave transitions in the THz range. Current ESR spectroscopy remains limited at THz frequencies because of the weak sources used, which allow measurements of free-induction decay (FID) signals that are linearly proportional to the excitation magnetic field strength but not measurements of spin echoes<sup>6</sup> and other nonlinear signals. This eliminates the possibility of two-dimensional (2D) THz ESR spectroscopy which, like 2D ESR at lower frequencies, could provide extensive insight into spin interactions and dynamics. In some cases including most or all proteins, even linear FID ESR signals may not be measurable because the THz spectrum includes much stronger absorption features due to low-frequency motions of polar segments<sup>7</sup>. However, the fast dephasing of such motions ensures that they would not compete with nonlinear spin echo signals<sup>6</sup>. The extension of established, commercially available methodologies in multidimensional magnetic resonance spectroscopy to the THz frequency range will find a wide range of applications spanning multiple disciplines.

Collective spin excitations in materials with spin order such as FM and AFM phases have been studied with weak THz fields, revealing the magnon frequencies through their FID signals<sup>8</sup> and demonstrating linear superposition in the responses to time-delayed pulse pairs<sup>8, 9</sup>. Nonlinear coherent control and spectroscopy could unravel complex spin interactions in AFM-to-FM order switching<sup>10</sup>, colossal magnetoresistance<sup>11</sup>, and multiferroicity<sup>12</sup>, and could enable new applications in quantum computing<sup>13</sup>, nonvolatile memory<sup>14</sup> and spintronics<sup>15</sup> at unprecedented fast time scales<sup>16, 17</sup>. THz nonlinear spectroscopy and coherent control have been demonstrated recently in various phases, almost exclusively utilizing THz electric fields<sup>18</sup>. So far there are very limited examples of nonlinear THz driving of spins<sup>19</sup> and none in which distinct nonlinear responses are separated from linear responses and from each other as is typical in 2D magnetic resonance spectroscopy. Here we explore the nonlinearity of magnons using time-delayed THz pulse pairs

with magnetic field strengths in excess of 0.1 tesla. We develop 2D THz magnetic resonance spectroscopy which can be understood in terms of multiple field-spin interactions that generate the nonlinear signal fields, similar to conventional 2D magnetic resonance but in the low-order perturbative regime more typical of 2D optical spectroscopies. Magnons are resonantly excited without promoting electrons to excited states (as in most spintronics excitation) and hence the observed nonlinearities are of purely magnetic origins.

The material under study is YFeO<sub>3</sub> (YFO). The ground state has canted AFM order<sup>8, 20</sup> with a net magnetization as shown in Fig. 1a. Two THz-active magnon modes, the quasi-AFM (AF) and quasi-FM (F) modes, can be constructed based on different cooperative motions of sublattice spins. Macroscopically the AF mode corresponds to oscillation of the magnetization amplitude and the F mode to precession of the magnetization orientation. In YFO at room temperature, the AF mode at frequency  $f_{\text{AF}} = 0.527$  THz and the F mode at  $f_{\text{F}} = 0.299$  THz can be selectively excited by THz pulses with magnetic field polarizations parallel and perpendicular respectively to the net magnetization direction. Upon THz excitation, magnons radiate FID signals  $\mathbf{B}(t)$  at their resonance frequencies, revealing the linear-response spin dynamics in the material. We measured the FID signal fields through time-dependent electro-optic sampling (EOS) as described in the Methods section. The linear measurements yielded the data shown in Figs. 1b and 1c.

Figure 2 shows the schematic experimental geometry. Two collinearly propagating single-cycle THz magnetic fields  $\mathbf{B}_A$  and  $\mathbf{B}_B$  were focused onto the sample. Incrementing the time delay  $\tau$  between the two excitation pulses, at each delay we recorded the coherent time-dependent signal field  $\mathbf{B}(\tau, t)$  emerging from the sample by EOS. We implemented a differential chopping detection scheme<sup>20</sup> (see Methods and Supplementary Information) to isolate the nonlinear signal resulting from magnons interacting with both THz pulses. The nonlinear signal field  $\mathbf{B}_{\text{NL}}$  is expressed as

$$\mathbf{B}_{\text{NL}}(\tau, t) = \mathbf{B}_{\text{AB}}(\tau, t) - \mathbf{B}_A(\tau, t) - \mathbf{B}_B(t), \quad (1)$$

where  $\mathbf{B}_{\text{AB}}$  is the signal with both THz pulses present, and  $\mathbf{B}_A$  and  $\mathbf{B}_B$  are signals with THz pulse A and B present individually. The experimental nonlinear 2D time-domain traces  $\mathbf{B}_{\text{NL}}$  for each magnon mode in YFO are displayed in Figs. 2c and 2d. Oscillations along the  $\tau$  axis reveal the dependence of the nonlinear signal on particular frequency components of the incident THz fields, and oscillations along the  $t$  axis reveal the frequency components in the nonlinear signal field. 2D Fourier transformation with respect to  $\tau$  and  $t$  yields 2D spectra as functions of excitation frequency  $\nu$  and detection frequency  $f$  as shown in Figs. 3a and 3c for each magnon mode. The difference in

phase accumulation of the induced magnon coherence during time periods  $\tau$  and  $t$  allows the 2D spectra to be separated into nonrephasing (NR) and rephasing (R) quadrants with correspondingly positive and negative excitation frequencies. Along zero excitation frequency there is a pump-probe (PP) spectral peak which results from THz-field-induced magnon population without phase accumulation.

The 2D spectrum for each magnon mode shows the complete set of third-order nonlinear signals. The R (spin echo<sup>6</sup>) peak and NR peak each result from a single field interaction during pulse A that creates a first-order magnon coherence and, after delay  $\tau$ , two field interactions during pulse B that generate a magnon population and then a third-order magnon coherence (either phase-reversed or not relative to the first-order coherence) that radiates the nonlinear signal. The 2-quantum (2Q) peak arises from two field interactions during pulse A that create a 2-quantum coherence (2QC) and, after time  $\tau$ , one field interaction during pulse B that induces transitions to a third-order 1-quantum coherence that radiates the signal. The 2QC reveals correlations between pairs of zone-center magnons<sup>22</sup> (distinct from zone-boundary magnon correlations revealed in 2-magnon Raman spectra<sup>23</sup>). The pump-probe signal is generated by two field interactions during pulse A that create magnon population and, after delay  $\tau$ , one interaction with pulse B that generates a third-order coherence that radiates the signal. These spectral peaks due to three field-magnon interactions are represented concisely by the Feynman pathways shown in the diagrams (i)-(iv) in Fig. 4a. In addition, second-order spectral peaks due to THz second harmonic generation and THz rectification are also identified in the AF mode 2D spectrum. The corresponding Feynman pathways are shown in diagrams (v)-(vi) in Fig. 4b. Second-order nonlinear processes are ordinarily forbidden in a centrosymmetric crystal, but are allowed in YFO due to time-reversal symmetry-breaking by the magnetic order.

To gain further insight into the underlying physics we performed simulations based on the Landau-Lifshitz-Gilbert (LLG) equation (see Supplementary Information). The Hamiltonian<sup>7,24</sup> is written as

$$H = J\mathbf{S}_1 \cdot \mathbf{S}_2 + \mathbf{D} \cdot (\mathbf{S}_1 \times \mathbf{S}_2) - \sum_{i=1}^2 (K_x S_{ix}^2 + K_z S_{iz}^2) - \gamma(\mathbf{B}_A(\tau, t) + \mathbf{B}_B(t)) \cdot \sum_{i=1}^2 \mathbf{S}_i. \quad (2)$$

The first term describes the AFM coupling between neighboring spins  $\mathbf{S}_1$  and  $\mathbf{S}_2$  with a positive exchange constant  $J$ . The second term derives from the Dzyaloshinskii-Moria (DM) interaction with the antisymmetric exchange parameter  $\mathbf{D}$  being a vector. The interplay between them results in the canted AFM ground state. The third term accounts for the crystalline anisotropy. The last

term is the Zeeman interaction between spins and THz magnetic fields. Numerically solving the LLG equation, we obtained vectorial solutions of the net magnetization  $\mathbf{M} \propto \mathbf{S}_1 + \mathbf{S}_2$  at different THz magnetic field polarizations. We extracted the nonlinear temporal responses of  $|\mathbf{M}|$  and  $M_x$  or  $M_y$  representing the AF and F mode magnons respectively. 2D Fourier transformation yielded the simulated 2D spectra of each magnon shown in Figs. 3b and 3d, exhibiting excellent agreement with the experimental results and confirming their magnetic origins. Comparing simulations with and without the DM interaction (i.e. canted AFM ground state versus AFM ground state), we found that the second-order responses of the AF mode were much stronger with the DM term, which conforms to the fact that the second-order nonlinearity resulting from time-reversal symmetry-breaking is mediated by the net magnetization from the canted AFM order. The second-harmonic and rectification signals are due to large-angle spin precessions<sup>25</sup>. Rectification signals have not been observed before. The connection between second harmonic and 2Q signals, which derive from the same 2-magnon coherences, is also newly observed. Further discussion of these signals is presented in the Supplementary Information.

We have demonstrated 2D magnetic resonance spectroscopy of THz-frequency magnons and directly observed nonlinear spin responses. The method is readily generalizable to other THz-frequency magnetic resonances such as spin transitions in molecular complexes and biomolecules with high ZFS. The methodology enables study of coupled degrees of freedom in various materials utilizing both the magnetic and electric fields of THz pulses. Further enhancement of the THz magnetic field by novel THz sources<sup>26</sup>, magnetic metamaterials<sup>18</sup> and resonant cavities may reveal magnetic and coupled nonlinearities beyond the perturbative limit and enable THz coherent control over magnetic domain orientation<sup>27</sup>, with promising applications in magnon spintronics<sup>15</sup>.

## Methods

**Experimental setup.** The laser we used was a Ti:Sapphire amplifier system (Coherent Inc.) operating at 1 kHz repetition rate with an output power of 4 W, delivering pulses at 800 nm with 100 fs duration. 95% of the laser output was split equally into two optical paths with a controlled time delay  $\tau$  between them. The optical pulses were recombined in a lithium niobate crystal to generate two single-cycle THz pulses by optical rectification utilizing the tilted-pulse-front technique<sup>28, 29</sup>. The two time-delayed, collinearly propagating THz pulses were collimated and focused by a pair of 90-degree off-axis parabolic mirrors, resulting in field strength in excess of 0.3 MV/cm for each pulse at the sample surface. The transmitted THz fields and FID signals were collimated and refocused into a 2 mm ZnTe electro-optic (EO) crystal by another pair of parabolic mirrors. The remaining 5% of the laser pulse energy was variably delayed by  $t$  with respect to THz pulse B and overlapped with the THz fields in the EO crystal. The time-dependent magnetic field profiles  $B(t)$  of the THz signals were measured through the time-dependent optical birefringence induced by their associated electric fields  $E(t)$  in the EO crystal, i.e. through EOS.

**Differential chopping detection.** We used two optical choppers both at a frequency of 250 Hz to modulate the two delayed optical pulses for THz generation. As shown in the Supplementary Materials Fig. S2, in successive laser shots there was generation of both THz pulses; pulse A only; pulse B only; and neither pulse. With background noise subtraction and averaging over 100 laser shots for each data point, the sensitivity of the experiment was approximately  $10^{-4}$ . The choppers and laser were synced to a DAQ card (National Instruments) which measured the signal from EOS<sup>30</sup>.

**Sample details.** The YFO sample was a 2 mm thick single crystal grown by the floating-zone method. The sample was (100) oriented with the crystal *c*-axis in the surface plane as verified by x-ray Laue diffraction.

## References

- 1 Bajaj, V.S. *et al.* Functional and shunt states of bacteriorhodopsin resolved by 250 GHz dynamic nuclear polarization-enhanced solid-state NMR. *Proc. Natl. Acad. Sci. USA* **106**, 9244-9249 (2009).
- 2 Borbat, P.P. *et al.* Electron spin resonance in studies of membranes and proteins. *Science* **291**, 266-269 (2001).
- 3 Koopens, F.H.L. *et al.* Driven coherent oscillations of a single electron spin in a quantum dot. *Nature* **442**, 766-771 (2006).
- 4 Craig, G.A. and Murrie, M. 3d single ion magnets. *Chem. Soc. Rev.* **44**, 2135 (2015).
- 5 Nehrkorn, J. *et al.* Zero-field splittings in metHb and met Mb with aquo and fluoro ligands: a FD-FT THz-EPR study. *Mol. Phys.* **111**, 269602707 (2013).
- 6 Hahn, E.L. Spin echo. *Phys. Rev.* **80**, 580 (1950).
- 7 Acbas, G., Niessen, K.A., Snell, E.H. and Markelz, A.G. Optical measurements of long-range protein vibrations. *Nature Comm.* **5**, 3076 (2014).
- 8 Yamaguchi, K., Nakajima, M. and Suemoto, T. Coherent control of spin precession motion with impulsive magnetic fields of half-cycle terahertz radiation. *Phys. Rev. Lett.* **105**, 237201 (2010).
- 9 Kampfrath, T. *et al.* Coherent terahertz control of antiferromagnetic spin waves. *Nature Photon.* **5**, 31-34 (2011).
- 10 Li, T. *et al.* Femtosecond switching of magnetism via strongly correlated spin-charge quantum excitations. *Nature* **496**, 69-73 (2013).
- 11 Rini, M. *et al.* Control of the electronic phase of a manganite by mode-selective vibrational excitation. *Nature* **449**, 72-74 (2007).
- 12 Eerenstein, W., Mathur, N.D. and Scott, J.F. Multiferroic and magnetoelectric materials. *Nature* **442**, 759-765 (2006).
- 13 Simon, J. *et al.* Single-photon bus connecting spin-wave quantum memories. *Nature Phys.* **3**, 765-769 (2007).
- 14 Lambert, C.H. *et al.* All-optical control of ferromagnetic thin films and nanostructures. *Science* **345**, 1337-1340 (2014).
- 15 Chumak, A.V., Vasyuchka, V.I., Serga, A.A. and Hillebrands, B. Magnon spintronics. *Nature Phys.* **11**, 453-461 (2015).
- 16 Kimel, A.V. *et al.* Inertia-driven spin switching in antiferromagnets. *Nature Phys.* **5**, 727-731 (2009).
- 17 Wienholdt, S., Hinzke, D. and Nowak, U. THz switching of antiferromagnets and ferrimagnets. *Phys. Rev. Lett.* **108**, 247207 (2012).
- 18 Kampfrath, T., Tanaka, K. and Nelson, K.A. Resonant and nonresonant control over matter and light by intense terahertz transients. *Nature Photon.* **7**, 680-690 (2013).
- 19 Mukai, Y. *et al.* Nonlinear magnetization dynamics of antiferromagnetic resonance induced by intense terahertz magnetic fields. *New J. Phys.* **18**, 013045 (2016).
- 20 Lütgemeier, H., Bohn, H.G. and Brajczewska, M. NMR observation of the spin structure and field induced spin reorientation in YFeO<sub>3</sub>. *J. Magn. Magn. Mater.* **21**, 289-296 (1980).
- 21 Woerner, M. *et al.* Ultrafast two-dimensional terahertz spectroscopy of elementary excitations in solids. *New J. Phys.* **15**, 025039(2013).

- 22 Morello, A., Stamp, P.C.E. and Tupitsyn, I.S. Pairwise decoherence in coupled spin qubit networks. *Phys. Rev. Lett.* **97**, 207206 (2006).
- 23 Fleury, P.A. and Loudon, R. Scattering of light by one- and two-magnon excitations. *Phys. Rev.* **166**, 514 (1968).
- 24 Herrmann, G.F. Resonance and high frequency susceptibility in canted antiferromagnetic substances. *J. Phys. Chem. Solids* **24**, 597-606 (1963).
- 25 Kiselev, S.I. et al. Microwave oscillations of a nanomagnet driven by a spin-polarized current. *Nature* **425**, 380-383 (2003).
- 26 Shalaby, M. and Hauri, C.P. Demonstration of a low-frequency three-dimensional terahertz bullet with extreme brightness. *Nature Commun.* **6**, 5976 (2015).
- 27 Baek, S.H. et al. Ferroelastic switching for nanoscale non-volatile magnetoelectric devices. *Nature Mater.* **9**, 309-314 (2010).
- 28 Yeh, K.-L. et al. Generation of 10  $\mu$ J ultrashort terahertz pulses by optical rectification. *Appl. Phys. Lett.* **90**, 171121 (2007).
- 29 Hirori, H. et al. Single-cycle terahertz pulses with amplitudes exceeding 1 MV/cm generated by optical rectification in LiNbO<sub>3</sub>. *Appl. Phys. Lett.* **98**, 091106 (2011).
- 30 Werley, C.A., Teo, S.M. and Nelson, K.A. Pulsed laser noise analysis and pump-probe signal detection with a data acquisition card, *Rev. Sci. Instrum.* **82**, 123108 (2011).

## **Acknowledgements**

This work was supported in part by Office of Naval Research Grant No. N00014-13-1-0509, National Science Foundation Grant No. CHE-1111557, and the Samsung GRO program. We thank Robert G. Griffin, Mei Hong, Thach Van Can, Prasahnt Sivarajah, Samuel W. Teitelbaum, Colby P. Steiner and Yongbao Sun for stimulating discussions.

## **Author contributions**

K.A.N., H.Y.H and J.L. conceived the experimental idea. H.Y.H. and J.L. designed the experiment. J.L. collected and analyzed the data. X.L. performed numerical simulation and assisted with experiment. B.K.O.-O. wrote the LabView code for data acquisition. H.Y.H. and B.K.O.-O. contributed to the modeling and data analysis. T.K. and T.S. prepared the sample and characterized the sample orientation. K.A.N. supervised the project. All authors contributed to understanding of the underlying physics and writing the manuscript.

## **Author Information**

The authors declare no competing financial interests. Correspondence and requests for materials should be addressed to K.A.N. (kanelson@mit.edu).

## Figures and legends

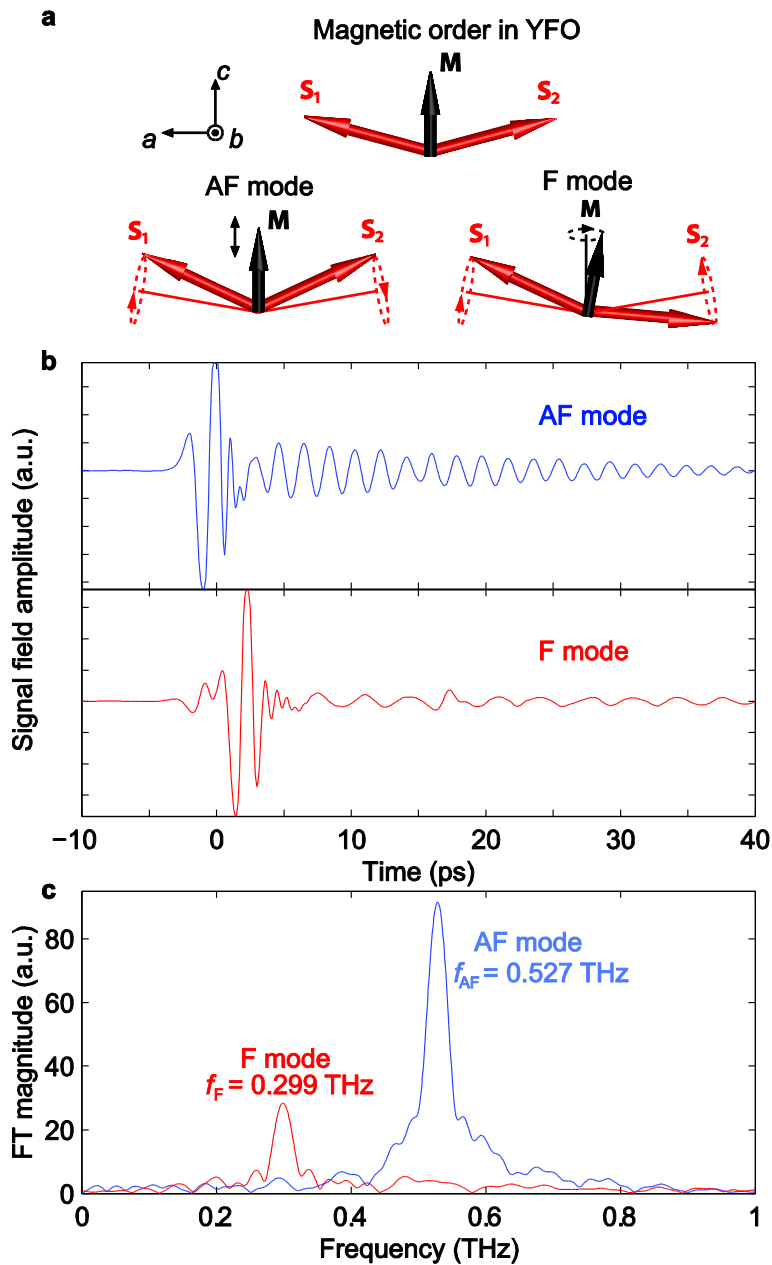


**Figure 1 | THz magnetic resonance of magnons in YFO.** **a**, The canted AFM order in YFO leads to a net magnetization  $\mathbf{M}$  along the crystal  $c$ -axis.  $\mathbf{S}_1$  and  $\mathbf{S}_2$  are the  $\text{Fe}^{3+}$  electron spins ordered along the crystal  $a$ -axis. The AF mode is the amplitude oscillation of  $\mathbf{M}$  while the F mode the precession of  $\mathbf{M}$ . **b**, Single THz pulses transmitted through the sample followed by FID signals from the AF (blue) and F (red) modes. **c**, Fourier transform magnitude spectra of the FID signals from the AF and F modes, showing magnon resonances at  $f_{\text{AF}} = 0.527 \text{ THz}$  and  $f_{\text{F}} = 0.299 \text{ THz}$ .

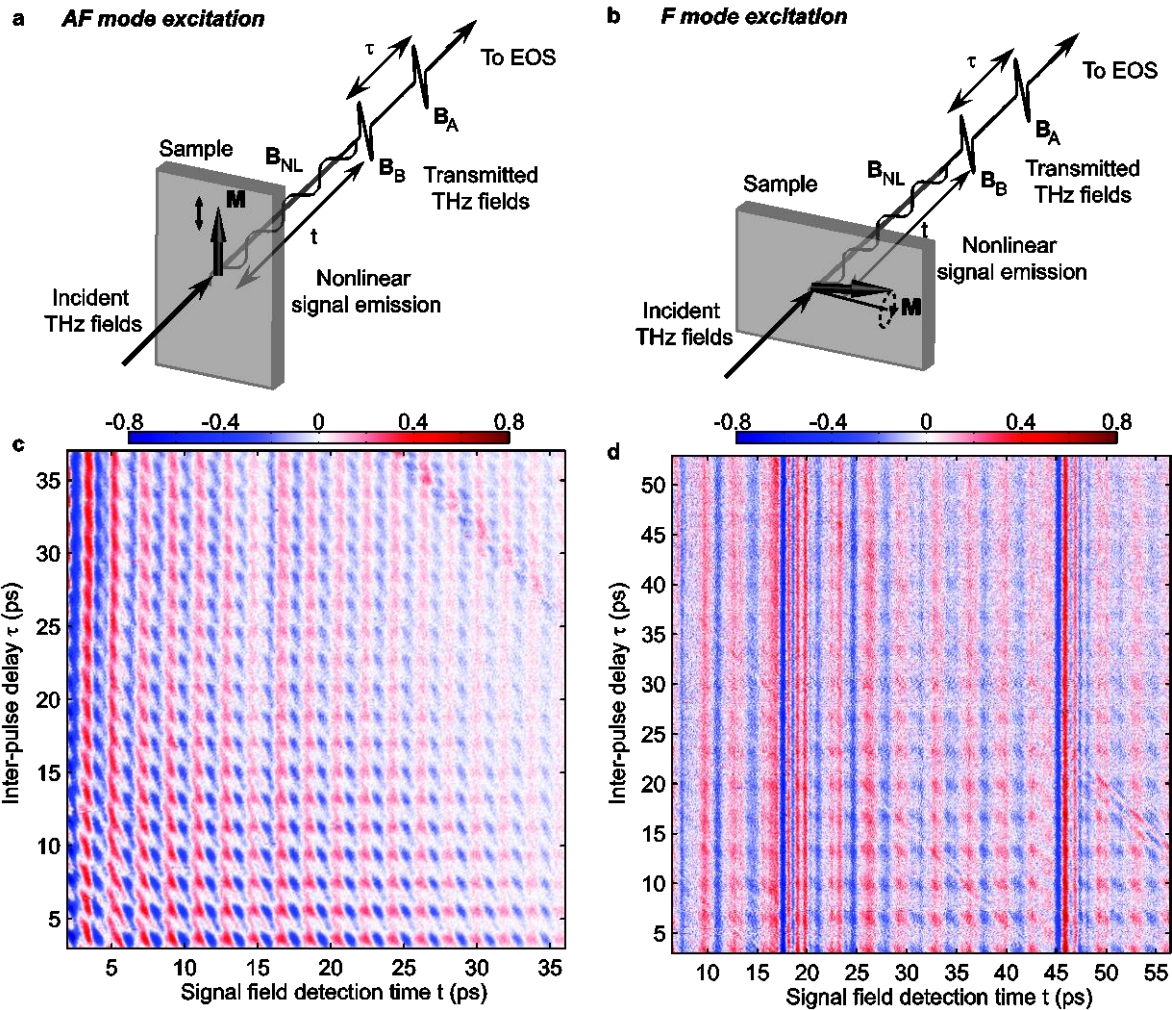


**Figure 2 | 2D THz time-domain spectroscopy.** **a** and **b**, Schematic illustrations of experimental geometry. Two THz pulses delayed by  $\tau$  with magnetic polarization parallel or perpendicular to the sample magnetization direction  $\mathbf{M}$  excite the AF (**a**) or F (**b**) mode respectively. At each inter-pulse delay  $\tau$ ,  $\mathbf{B}_{\text{NL}}(\tau, t)$  copolarized with input THz magnetic fields is measured by EOS as a function of  $t$ . **c** and **d**, Normalized 2D time-time plots of  $\mathbf{B}_{\text{NL}}(\tau, t)$  from the AF (**c**) and F (**d**) mode respectively. Amplitudes exceeding  $\pm 0.8$  are saturated in the colormap.

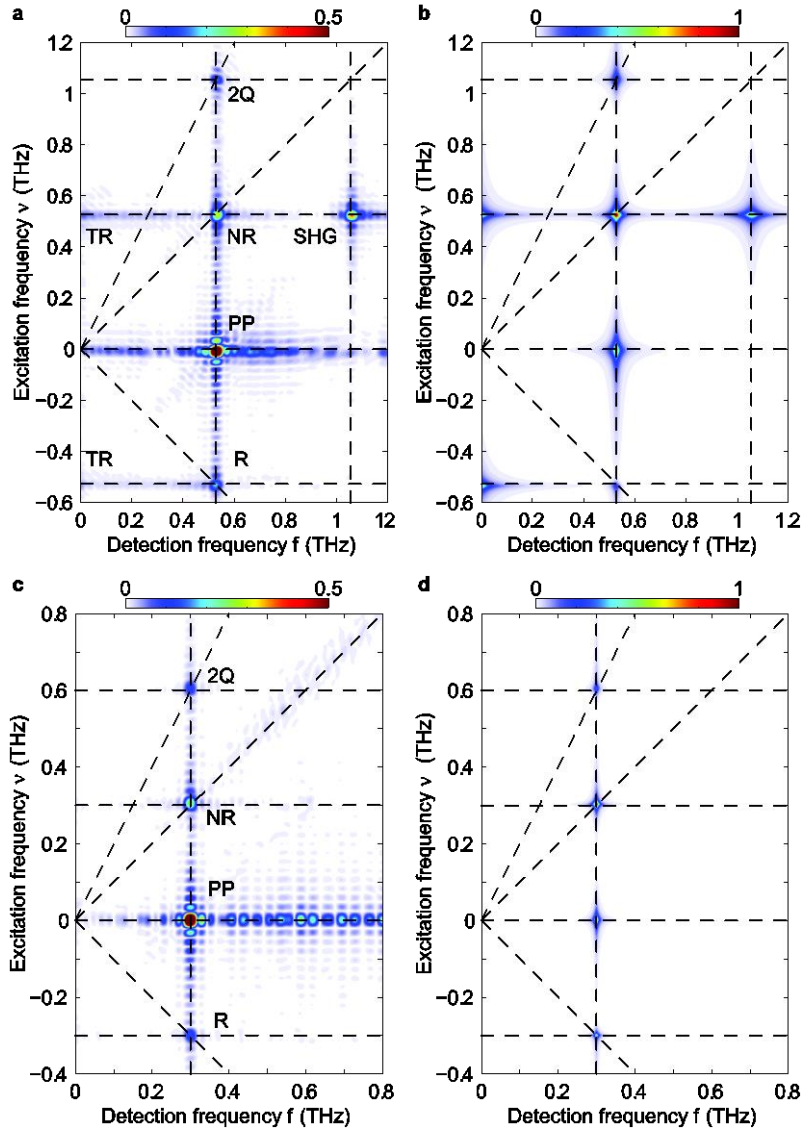


**Figure 3 | 2D magnetic resonance spectra of magnons in YFO.** **a** and **b**, Experimental (**a**) and simulated (**b**) AF mode 2D magnitude spectra. Third-order spectral peaks include pump-probe (PP), nonrephasing (NR) rephasing (R) and 2-quantum (2Q) peaks. Second-order peaks include second harmonic generation (SHG) and THz rectification (TR) peaks. **c** and **d**, Experimental (**c**) and simulated (**d**) F mode 2D magnitude spectra showing the full set of third-order peaks. All spectra are normalized and plotted according to the color scale shown. Real and imaginary signals at selected frequency components are shown in the Supplementary Information Fig. S4.

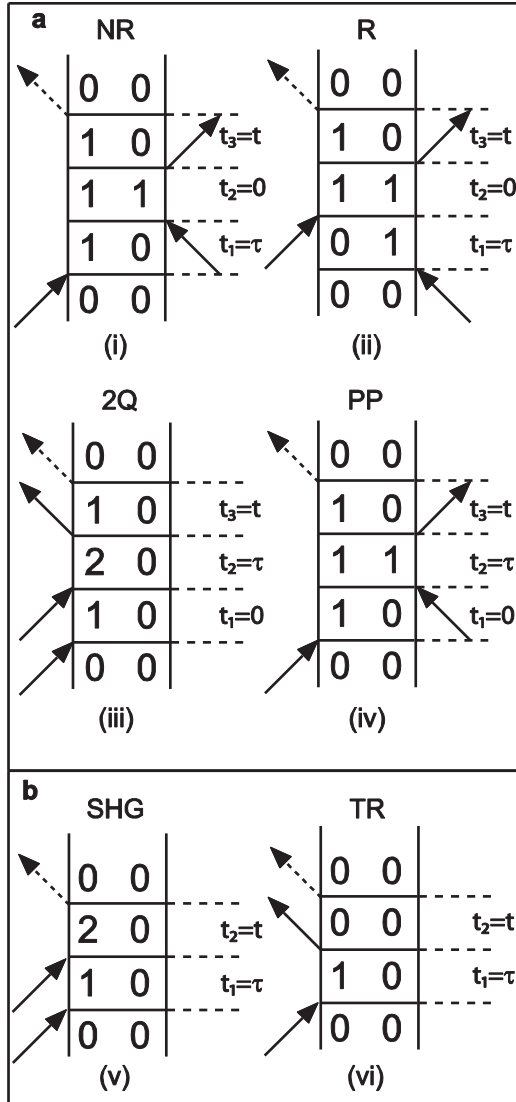


**Figure 4 | Double-sided Feynman diagrams.** **a** and **b**, Double-sided Feynman diagrams show typical excitation pathways leading to the coherent emission of third-order (**a**, (i)-(iv)) and second-order (**b**, (v)-(vi)) nonlinear signals. Each solid arrow denotes a field interaction that induces a transition between magnon populations or coherences denoted by diagonal ( $|0\rangle\langle 0|$ ,  $|1\rangle\langle 1|$ ) or off-diagonal ( $|1\rangle\langle 0|$ ,  $|2\rangle\langle 0|$ ) density matrix elements respectively. The dashed arrows represent the measured signal fields. The time interval subscripts denote the number of preceding field interactions.